USGS
science for a changing world
U.S. DEPARTMENT OF THE INTERIOR
U.S. GEOLOGICAL SURVEY

Prepared for the
NATIONAL AERONAUTICS AND SPACE ADMINISTRATION

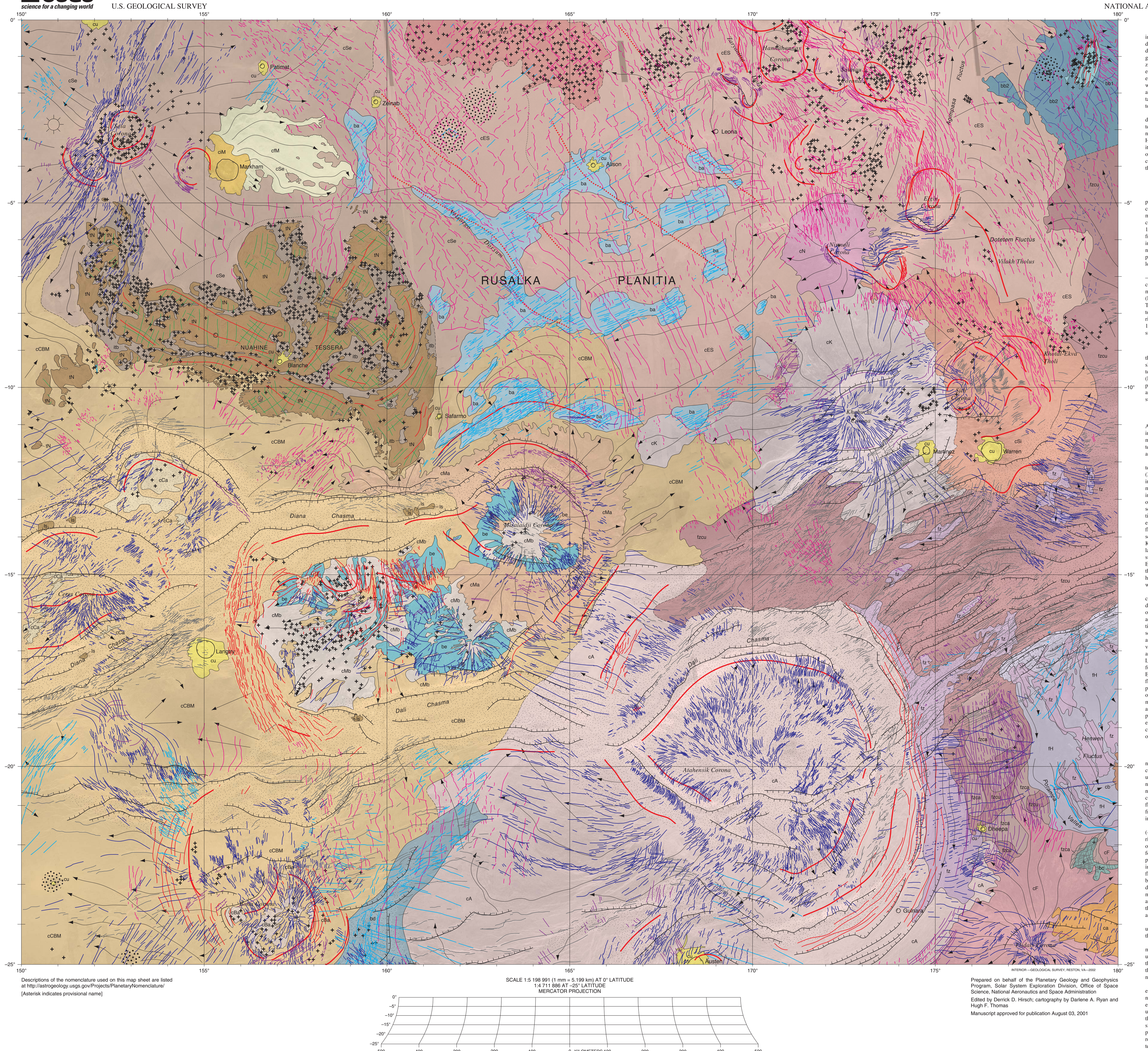

Descriptions of the nomenclature used on this map sheet are listed at http://astrogeology.usgs.gov/Projects/PlanetaryNomenclature/

[Asterisk indicates provisional name]

SCALE 1:5 198 991 (1 mm = 5.199 km) AT 0° LATITUDE
1:4 711 886 AT –25° LATITUDE
MERCATOR PROJECTION

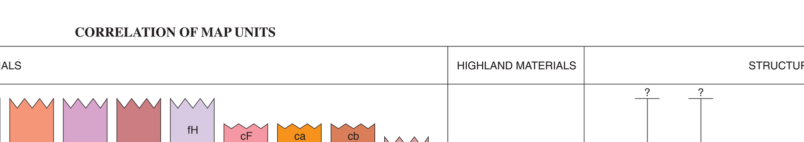

Prepared on behalf of the Planetary Geology and Geophysics Program, Solar System Exploration Division, Office of Space Science, National Aeronautics and Space Administration

Edited by Derrick D. Hirsch; cartography by Darlene A. Ryan and Hugh F. Thomas

Manuscript approved for publication August 03, 2001

CORRELATION OF MAP UNITS

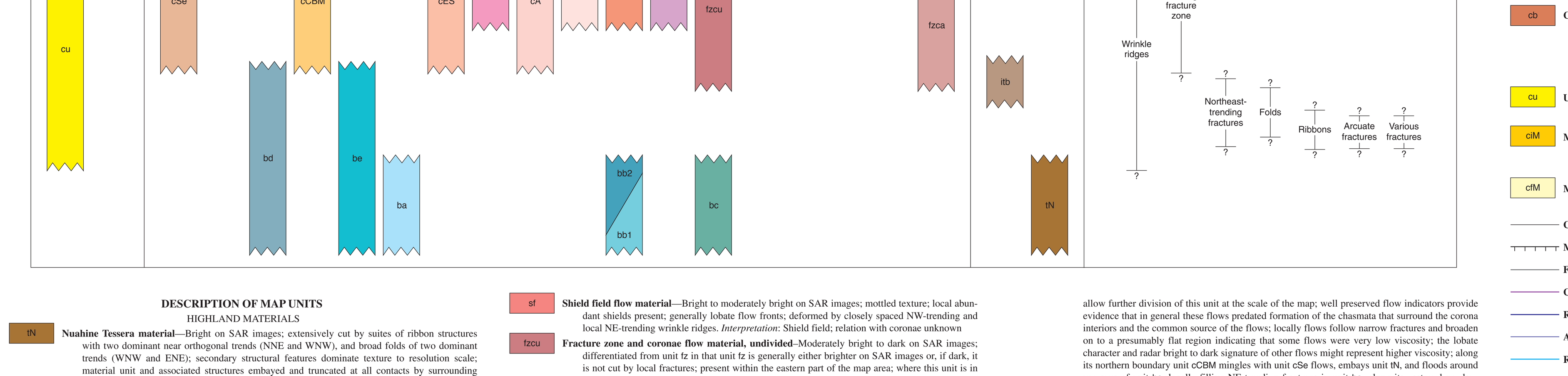

DESCRIPTION OF MAP UNITS

HIGHLAND MATERIALS

tN **Nuahine Tessera material**—Bright on SAR images; extensively cut by suites of ribbon structures with two dominant near orthogonal trends (NNE and WNW), and broad folds of two dominant trends (WNW and ENE); secondary structural features dominate texture to resolution scale; material unit and associated structures embayed and truncated at all contacts by surrounding material; occurs as one large isolated inlier. *Interpretation*: Extensively deformed ribbon and fold structures and patterns similar to extended ribbon-fold terrain (Hansen and Willis, 1996, 1998) and to the marginal fold belt domain of crustal plateaus (Ghent and Hansen, 1999); base material unit of unknown origin

itb **Intratessera basin material**—Dark on SAR images; hosts abundant shield edifices; embays ribbon and fold basins in tessera terrain. *Interpretation*: Low viscosity lava flows associated with tessera terrain formation and crustal plateau evolution (for example, Banks and Hansen, 2000; Hansen and others, 1999)

CORONAE AND PLANITIA MATERIALS

[Planitia materials: Radar dark to bright, homogeneous to inhomogeneous, mottled to smooth flow units; smooth to digitate to lobate flow fronts; undeformed to variably deformed by suites of fractures, folds, or warps. Coronae materials: Homogeneous to inhomogeneous, mottled to smooth, digitate to lobate flow fronts; variably deformed by suites of concentric fractures, radial fractures, and margin folds (or all) related to local coronae; deformation intensity varies from corona to corona; individual flow fronts or lobes may appear more radar bright than the host unit due to local changes in surface roughness]

ba **Basal material, unit a**—Dark on SAR images; hosts abundant NE- to ENE-trending fractures; deformed by NNW-trending wrinkle ridges throughout; forms local topographic highs; fractures truncated by overlying Eigin and Saunau Coronae flow material (unit cES). *Interpretation:* One of the oldest units in the south Rusalka Planitia; age relative to tessera deformation and tessera host is unconstrained; fractured lava flows

bb1 **Basal material, unit b, member 1**—Bright on SAR images; contains shields (ages of which are unknown); deformed by N-trending folds (for example, Stofan and others, 1993). Reference locality: 1° S., 178.5° E. *Interpretation*: Lava flows of unknown age; unit bb1 emplacement continued with continued fold formation

bb2 **Basal material, unit b, member 2**—Dark on SAR images; deformed by paired arcuate fractures that terminate in broad "V" or as "T" termination with other fractures; hosts abundant short NNW-trending wrinkle ridges; embays fold axes of fold belt, yet is itself involved in folding; present in northeast corner of map area. *Interpretation*: Lava flows of unknown age; predates adjacent coronae-related lava flows (unit cES); folding predates and postdates unit bb2 emplacement; arcuate fractures postdate unit bb2 emplacement

bc **Basal material, unit c**—Bright on SAR images; cut by NS-, NE-, and EW-trending fractures; preserved as a local topographic high; locally flows of unit cF follow fractures in unit bc. Reference locality: 22.5° S., 179° E. *Interpretation*: Lava flows of unknown age; predates adjacent coronae-related lava flows (unit cF), could include some flows from Atahensik Corona

bd **Basal material, unit d**—Bright to moderately dark on SAR images; cut by fractures of many orientations as well as fracture zone related faults; preserved as a local topographic high; locally flows of units cA and cCBM follow fractures in unit bc; hosts NS-trending wrinkle ridges. Reference locality: 22.5° S., 161° E. *Interpretation*: Lava flows of unknown age; predates adjacent coronae-related lava flows (unit cCBM)

be **Basal material, unit e**—Generally bright on SAR images; cut by structural fabric reflecting many orientations, brightness may also locally relate to flow surfaces; preserved in the interior of Miralaidji Corona complex. *Interpretation*: Variably deformed to undeformed lava flows of unknown age—this unit could variably represent surfaces that predate Miralaidji Corona or could represent early volcanic or tectonic facies related to Miralaidji formation; predates to temporally overlaps with adjacent coronae-related lava flows (unit cCBM)

sf **Shield field flow material**—Bright to moderately bright on SAR images; mottled texture; local abundant shields present; generally lobate flow fronts; deformed by closely spaced NW-trending and local NE-trending wrinkle ridges. *Interpretation*: Shield field; relation with coronae unknown

fzcu **Fracture zone and coronae flow material, undivided**–Moderately bright to dark on SAR images; differentiated from unit fz in that unit fz is generally either brighter on SAR images or, if dark, it is not cut by local fractures; present within the eastern part of the map area; where this unit is in contact with unit fz, it is older based on the presence of fractures in unit fzcu and absence of those same fractures in unit fz along fracture strike; however, broad temporal relations with respect to unit fz are unconstrained. *Interpretation*: Conglomeration of lava flows erupted from fractures associated with the NE-trending fracture zone and from coronae (the most prominent sources within V–38 quadrangle to the east)

fzca **Fracture zone and coronae flow material, unit a**–Moderately dark on SAR images; hosts local shields; differentiated from unit fz in that unit fz is brighter on SAR images; present within the eastern part of the map area; where this unit is in contact with unit fzcu, it is generally younger based on the presence of fractures in unit fzcu and absence of those same fractures in unit fzca along fracture strike; however, broad temporal relations with respect to unit fzcu are unconstrained; unit fzca is also younger than unit bc, as unit bc preserves a record of older fracture suites; unit fzca is older than units cF and fH where in contact with these units. *Interpretation*: Conglomeration of lava flows erupted from any of three sources: fractures associated with the NE-trending fracture zone, coronae, or undefined sources

fz **Fracture zone flow material**—Very bright to dark on SAR images; lobate to digitate flow fronts; locally cut by pervasive NE-trending fractures and faults within the fracture zone region. *Interpretation*: Conglomeration of lava flows erupted from fractures associated with the NE-trending fracture zone

fH **Henwen Fluctus flow material**—Very bright to dark on SAR images; lobate to digitate flow fronts; channels, levees, breached levees, and well preserved flow indicators are consistent with broadly synchronous flow of variable roughness. Flows emanate from the NE-fracture zone system yet are cut by fractures of this same system; unit fH postdates adjacent units fzcu and fzca and probably locally postdates adjacent unit cF flows although broad temporal relations with respect to unit cF are unconstrained, as are temporal relations with unit cb. *Interpretation*: Conglomeration of lava flows erupted from fractures associated with the NE-trending fracture zone

cES **Eigin and Saunau Coronae flow material, undivided**—Moderately bright to moderately dark on SAR image; irregular to subdued lobate to nonlobate flow fronts; distal parts of flows are darker in SAR than proximal parts of flows; lobate character best preserved in proximal locations; locally cut by wrinkle ridges and fractures related to individual coronae; locally superimposed on unit ba as evidenced by local filling by unit cES of fractures that cut unit ba; includes Argimpasa Fluctus and Dotetem Fluctus. *Interpretation*: Lava flows derived from multiple coronae, including Eigin and Saunau; low viscosity lava flows emplaced following preexisting topography, yet locally uplifted following emplacement

cSe **Seia Corona flow material**—Moderately dark to moderately bright on SAR images; includes flows from Seia Corona; shields locally present in the northwest (possibly related to Seia Corona); cut by NE-trending fractures associated with Seia Corona; localized NE-trending wrinkle ridges present in the southeast; locally fills moat around tessera inlier and locally embays tessera material; shows broadly synchronous temporal relations with unit cBM, and indeterminable temporal relations with unit cES. *Interpretation*: Conglomeration of lava flows related to Seia Corona

cCBM **Ceres, Bona, and Miralaidji Coronae flow material, undivided**—Bright to dark on SAR images; includes digitate to lobate to homogeneous to mottled flows from Ceres and Bona Coronae and from Miralaidji Corona complex; flow indicators mapped on the basis of lobate and digitate flow boundaries provide indications of local source regions; locally deformed by radial and concentric fractures and folds related to corona formation; intimate detailed relations between flows did not allow further division of this unit at the scale of the map; well preserved flow indicators provide evidence that in general these flows predated formation of the chasmata that surround the corona interiors and the common source of the flows; locally flows follow narrow fractures and broaden on to a presumably flat region indicating that some flows were very low viscosity; the lobate character and radar bright to dark signature of other flows might represent higher viscosity; along its northern boundary unit cCBM mingles with unit cSe flows, embays unit tN, and floods around upwarps of unit ba, locally filling NE-trending fractures in unit ba; along its eastern boundary unit cCBM shows mutually cross-cutting relations with units cK and fzcu; along its southeast boundary unit cCBM shows generally indeterminable temporal relations with unit cA; locally unit cCBM is deformed by broad NE warps concentric to Miralaidji Corona and to Atahensik Corona, indicating that some corona-related deformation outlasted some volcanism; to the south, unit cCBM flows up to and locally through fractures in unit cSC; this unit is widely variably deformed by corona-related structures and fracture zone structures. *Interpretation*: Lava flows related to Cere and Bona Coronae and to Miralaidji Corona complex

cCa **Ceres Corona flow material, unit a**—Radar dark on SAR images; shields locally present; fills local topographic lows in the central region of Ceres Corona with minor distribution in adjacent chasmata; locally fractured by corona-related fractures, but generally late with respect to the tectonic evolution of Ceres Corona. *Interpretation*: Late lava flows and shields related to Ceres Corona

cBa **Bona Corona flow material, unit a**—Radar dark on SAR images; shields locally present; fills local topographic lows in the central region of Bona Corona; locally fractured by corona-related fractures, but generally late with respect to the tectonic evolution of Bona Corona. *Interpretation*: Late lava flows and shields related to Bona Corona

cMa **Miralaidji Corona flow material, unit a**—Moderately radar bright to dark on SAR images; flow indicators mapped on the basis of lobate and digitate flow boundaries provide indications of local source regions; well preserved flow indicators provide evidence that in general these flows emanate from fractures that are either radial or concentric to central Miralaidji Corona; radial or concentric fractures locally deform the flows. *Interpretation*: Lava flows that emanate from dominantly concentric corona fractures related to Miralaidji Corona formation

cMb **Miralaidji Corona flow material, unit b**—Radar dark on SAR images; shields locally present; fills local topographic lows in the interior of Miralaidji Corona complex; locally fractured by corona-related fractures, but generally late with respect to the tectonic evolution of Miralaidji Corona complex. *Interpretation*: Late lava flows and shields related to Miralaidji Corona complex

cA **Atahensik Corona flow material**—Bright to dark on SAR images, variably deformed by corona-related radial and concentric fractures and folds; local digitate and lobate flows indicate flow direction (and hence source); flows can be cut by fractures, yet also emanate from parallel fractures, indicating broad synchroneity of Atahensik tectonism and magmatism; along the east side of Atahensik, unit cA generally predates adjacent unit fz; folded unit cA is locally embayed by unit fz (which is itself locally folded); the region of unit fzcu east of Atahensik may be contiguous with unit cA in the subsurface; west of Atahensik no consistent temporal relations with unit cCBM are discernable, indicating broad synchronicity of these composite flows; north of Atahensik, unit fzcu may include unit cA flows; the contact between these two units is drawn on the basis of radar brightness at this location which may or may not be correlative with specific flows. *Interpretation*: Lava flows related to Atahensik Corona

cSi **Sith Corona flow material**—Moderately bright on SAR images; cut by radial fractures and fold belt related to Sith Corona. *Reference locality*: 10.2° S., 176.5° E. *Interpretation*: Lava flows related to formation of Sith Corona

cK **Khabuchi Corona flow material**—Moderately bright to moderately dark on SAR images; lobate flow fronts; unit interior cut by radial fractures; centered at 10.6° S., 172.6° E. *Interpretation*: Lava flows from unnamed corona

cN **Nirmali Corona flow material**—Moderately bright to moderately dark on SAR images; highly digitate flow fronts; deformed by one suite of concentric fractures. *Reference locality*: 6.3° S., 172.3° E. *Interpretation*: Young lava flows derived from corona b

cF **Flidais Corona flow material**—Dark on SAR images; individual flows digitate; radial fractures and concentric scarps deform the interior; flows follow radial fractures, yet are also cut by radial fractures, indicating that Flidais tectonism and magmatism broadly overlapped in time. *Reference locality*: 24.5° S., 177.3° E. *Interpretation*: Lava flows related to formation of Flidais Corona with synchronous and subsequent deformation

ca **Corona a flow material**—Bright on SAR images; individual flows digitate; cut by radial fractures from Flidais Corona. *Reference locality*: 24° S., 179° E. *Interpretation*: Lava flows related to unnamed corona in southwest V–38 quadrangle

cb **Corona b flow material**—Bright on SAR images; individual flows digitate; along the easternmost boundary of map area near 20° S.; flows from another unnamed corona in V–38 quadrangle barely spill into map area. *Interpretation*: Lava flows related to unnamed corona in southwest V–38 quadrangle

CRATER MATERIALS

[Generally radar bright material associated with individual impact craters]

cu **Undifferentiated crater material**—Bright to moderately bright on SAR images; occur as flowlike deposits associated with impact craters. *Interpretation*: Deposits and structures created by meteorite impact, including impact melt, fluidized ejecta, or subsurface magma

ciM **Markham crater impact material**—Very bright to very dark (some floor materials) on SAR images; includes floor, central peak, wall, rim, interior flood lava materials, and ejecta blanket; texture granular to smooth. *Reference locality*: 4.1° S., 155.6° E. *Interpretation*: Deposits and structures created by meteorite impact

cfM **Markham crater flow material**—Moderately bright on SAR images; digitate eastern flow fronts. *Interpretation*: Impact melt or fluidized ejecta created by meteorite impact

Contact—Dashed where gradational or uncertain; dotted for possible contact

Major scarp—Ticks on down side

Fault or fracture—Generally associated with fracture zone

Concentric fracture—Associated with coronae

Radial fracture—Associated with coronae

Arcuate fracture—Associated with units bb2 and fzcu. Dashed where partly buried

Regional fracture—Dashed where partly buried

Fold crest

Broad ridge crest—Generally associated with coronae

Broad warp

Wrinkle ridge

Ribbon trends

Crater rim crest—Hachures when diameter greater than 20 km across; no hachures when diameter less than 20 km across

Small shields—Less than 10 km across

Large shield or dome—Greater than 10 km across

Channel

Fracture zone

Airburst spot

Lava flow direction

ls **Slide material**—Interpreted to be result of mass wasting along trench slope

The Magellan Mission

The Magellan spacecraft orbited Venus from August 10, 1990, until it plunged into the venusian atmosphere on October 12, 1994. Magellan had the objectives of (1) improving knowledge of the geologic processes, surface properties, and geologic history of Venus by analysis of surface radar characteristics, topography, and morphology and (2) improving knowledge of the geophysics of Venus by analysis of venusian gravity.

The Magellan spacecraft carried a 12.6-cm radar system to map the surface of Venus. The transmitter and receiver systems were used to collect three datasets: synthetic aperture radar (SAR) images of the surface, passive microwave thermal emission observations, and measurements of the backscattered power at small angles of incidence, which were processed to yield altimetric data. Radar imaging and altimetric and radiometric mapping of the venusian surface were done in mission cycles 1, 2, and 3, from September 1990 until September 1992. Ninety-eight percent of the surface was mapped with radar resolution of approximately 120 meters. The SAR observations were projected to a 75-m nominal horizontal resolution; these full-resolution data compose the image base used in geologic mapping. The primary polarization mode was horizontal-transmit, horizontal-receive (HH), but additional data for selected areas were collected for the vertical polarization sense. Incidence angles varied from about 20° to 45°.

High-resolution Doppler tracking of the spacecraft was done from September 1992 through October 1994 (mission cycles 4, 5, 6). High-resolution gravity observations from about 950 orbits were obtained between September 1992 and May 1993, while Magellan was in an elliptical orbit with a periapsis near 175 kilometers and an apoapsis near 8,000 kilometers. Observations from an additional 1,500 orbits were obtained following orbit-circularization in mid-1993. These data exist as a 75° by 75° harmonic field.

Magellan Radar Data

Radar backscatter power is determined by the morphology of the surface at a broad range of scales and by the intrinsic reflectivity, or dielectric constant, of the material. Topography at scales of several meters and larger can produce quasi-specular echoes, with the strength of the return greatest when the local surface is perpendicular to the incident beam. This type of scattering is most important at very small angles of incidence, because natural surfaces generally have few large tilted facets at high angles. The exception is in areas of steep slopes, such as ridges or rift zones, where favorably tilted terrain can produce very bright signatures in the radar image. For most other areas, diffuse echoes from roughness at scales comparable to the radar wavelength are responsible for variations in the SAR return. In either case, the echo strength is also modulated by the reflectivity of the surface material. The density of the upper few wavelengths of the surface can have a significant effect. Low-density layers, such as crater ejecta or volcanic ash, can absorb the incident energy and produce a lower observed echo. On Venus, a rapid increase in reflectivity exists at a certain critical elevation, above which high-dielectric minerals or coatings are thermodynamically stable. This effect leads to very bright SAR echoes from virtually all areas above that critical elevation.

The measurements of passive thermal emission from Venus, though of much lower spatial resolution than the SAR data, are more sensitive to changes in the dielectric constant of the surface than to roughness. As such, they can be used to augment studies of the surface and to discriminate between roughness and reflectivity effects. Observations of the near-nadir backscatter power, collected using a separate smaller antenna on the spacecraft, were modeled using the Hagfors expression for echoes from gently undulating surfaces to yield estimates of planetary radius, Fresnel reflectivity, and root-mean-square (rms) slope. The topography data produced by this technique have horizontal footprint sizes of about 10 km near periapsis and a vertical resolution of approximately 100 m. The Fresnel reflectivity data provide a comparison to the emissivity maps, and the rms slope parameter is an indicator of the surface tilts, which contribute to the quasi-specular scattering component.

INTRODUCTION

The Diana Chasma quadrangle (V–37), an equatorial region between 0º and 25º S. and 150º and 180º E. that encompasses ~8,400,000 km², is broadly divided into southern Rusalka Planitia in the north, eastern Aphrodite Terra in the central region, and unnamed regions to the south. Geologic mapping constrains the temporal and spatial relations of the major features, which include a tessera inlier, Markham crater, six large coronae (300–675 km diameter), four smaller coronae (150–225 km diameter), Diana and Dali chasmata, a large fracture zone, and southern Rusalka Planitia (fig. 1*A*, *B*). Eastern Aphrodite Terra, marked here by large coronae, deep chasmata, and an extensive northeast-trending fracture zone, extends from Atla Regio to Thetis Regio. The large coronae are part of a chain of such features that includes Inari Corona to the west-southwest and Zemina Corona to the northeast. V–37 quadrangle is bounded on the north by Rusalka Planitia and on the south by Zhibek Planitia. International Astronomical Union (IAU) approved and provisional nomenclature and positions for geographic features within Diana Chasma quadrangle are shown on the geologic map. [Note: Atahensik Corona was referred to as Latona Corona in much previously published literature.]

Diana Chasma quadrangle hosts some of the steepest topography on Venus. Altimetry measurements range from –2.5 to 4.7 km (0.0 = mean planetary radius), with a surface mean of 0.6 km (fig. 1*C*). Fractures and faults within the central fracture/rift zone create large blocks of down-dropped material, especially along the east-central edge of the map area. The Dali and Diana chasmata display slopes of >30° (fig. 1*D*), the steepest and deepest trenches on Venus (Ford and Pettengill, 1992). Both chasmata host landslide deposits presumably sourced from the steep chasmata walls. The tessera inlier, coronae, and ridge belts sit topographically above Rusalka and Zhibek planitiae. Rusalka Planitia topography describes broad undulations having northwest-trending ridges spaced ~200 km apart. The most distinctive ridge, Vetsorgo Dorsum, centered at 6.5° S., 163° E., is a Class I ridge belt (Kryuchkov, 1988; Banerdt and others, 1997) owing to its simple arch morphology. The central interior of Markham crater sits topographically lower than the surrounding region, which slopes downward to the east.

DATA SETS

Regional data sets are shown in figure 1. Detailed mapping was conducted using cycles 1, 2, and 3 Magellan synthetic aperture radar (SAR) images at CMIDR and FMIDR scale, and Magellan altimetry, emissivity, reflectivity, and slope data where available. FMAP's in both printed photo and CD-ROM format provided the highest image resolution to view complicated volcanic and tectonic contacts. Stereo images, generated using cycles 1 and 3 SAR stereo pairs (Plaut, 1993), and synthetic stereo images, generated using topography and cycle 1 SAR (Kirk and others, 1992), proved useful in resolving the interactions of flows, primary and secondary structures, and topography. Incidence angles in the map area provide a moderate range in viewing angle: cycle 1, 35.5°–45.2°; cycle 2, 24.9°–25.1°; cycle 3 stereo 24.5°–18.7°.

MAPPING TECHNIQUES

We began our mapping by compilation at CMIDR framelet scale using Magellan data and Adobe Illustrator 6.0®. At the time, FMIDR digital data was not available for much of the region. Use of IDL and Image software allowed interactive adjustment of image stretch for detailed mapping, a technique that is particularly critical for mapping subtle material unit and structural facies in the plains regions. Throughout the mapping we treated material units separate from tectonic (secondary) structures and delineated the spatial distribution of each (Hansen, 2000) in order to avoid the assumption that tectonic structures form at the same time as the material unit (typically volcanic).

Problems inherent to mapping in the Diana Chasma quadrangle include (1) radar artifacts related to extremes in topography (Ford and others, 1993), (2) highly deformed units no longer identifiable as distinct primary lithologies, and (3) difficulty in determining the limits of many corona flow units, as these units commonly show gradational changes in radar brightness. Many areas, including the chasmata, exhibit very high backscatter coefficients and radar layover, making identification of material units difficult. The primary material unit(s) deformed by the two main ridge belts, interiors of the larger coronae (that is, Ceres, Miralaidji, and Atahensik), and four discrete, locally deformed outcrops only locally exhibit individual volcanic flow fronts or other material characteristics that can be distinguished apart from secondary structures. As a result, these units are grouped together although such grouping is not meant to imply formation as a single coherent unit emplaced as a single event. The deformed material may comprise preexisting material, early-formed coronae-related lava flows, or other volcanic constructs. In all cases we refer to the material units as flows. We assume that Venus could host only the three basic rock types we observe on Earth: igneous, metamorphic, or sedimentary rocks. Owing to the lack of surface water and to the paucity of eolian erosion on Venus (for example, Kaula, 1990), large amounts of surface rocks are likely not of sedimentary origin. Furthermore, owing to the apparent lack of widespread erosion, surface rocks are not likely exposed crustal metamorphic or intrusive igneous rocks. Thus surface rocks most likely dominantly originated as extrusive igneous rocks, that is volcanic flows, or simply flows. Exceptions include impact-related, landslide, and eolian deposits. Although these deposits are locally present on Venus, they are areally minor. One might argue that sedimentary or metamorphic rocks exist on the surface of Venus, but we have come across no convincing evidence for widespread distribution of either of these two general rock types and we will consider them no further because of a lack of evidence for their presence.

Venus' geological units (or material units; for example, volcanic flows, eolian deposits, crater deposits) are typically differentiated in Magellan data by patterns in SAR, emissivity, [?/reflectivity] or root mean square (rms) slope data that reflect primary features such as lobate flows, mottling, or homogeneity (Ford and others, 1993). The first order task in mapping material units is to determine their spatial distribution and to examine contact relations between adjacent units (Wilhelms, 1990). Several problems must be kept in mind. Available data might inhibit unique distinction between different material units or may result in division of a single unit into two apparently different units (Hansen, 2000). For example, spatially separate lava flows may show similar radar, emissivity, or rms slope characteristics and hence one might conclude (incorrectly) that these units are time correlative. Alternatively, a single (or composite) volcanic flow unit emplaced within a single eruptive event may have different facies and show radically different radar and rms slope signatures, and therefore they might be interpreted (incorrectly) as temporally distinct geological units. Lumping versus splitting of material units depends in part on the understanding of process-dependent facies changes; fundamentally these potential problems are no different from those encountered in terrestrial mapping, although on Earth one may have more tools to address the problem. In an attempt to address these issues, in practice we indicate flow direction data on the map; these arrows indicate both the interpreted flow direction and location of flows, but also provide for the user an indication of where we believe that there is substantive evidence to indicate the minimum limits of flow units. Users might treat such data in the same way that strike and dip information is treated on terrestrial maps—as a clear indication that the data were collected and interpreted at those specific locations. That is, the density and location of strike and dip symbology clearly indicates to a user not only the orientation of specific units, but also provide evidence of where a mapper has actually traversed the ground, and where map relations are projected from elsewhere. Dashed lines indicate the uncertainly of unit contacts, or the gradational nature of unit contacts. In many cases the exact location of a unit contact is important only in the context of a specific question; thus we encourage users of this map to examine such contacts in detail with specific individual questions in mind.

MAJOR GEOLOGIC UNITS

The map area is dominated by several major units, including tessera terrain, corona-related flows, a shield-dominated unit, and a moderately regionally extensive unit that is cut by northeast-trending fractures and appears to underlie coronae-related flows within the northern portion of the map area and extending north to V–25 quadrangle. All of the units are variably cut by generally north- to north-northwest-trending wrinkle ridges. Structurally the region is dominated by radial and concentric fractures, faults, and folds associated with the many coronae, as well as a regional east-northeast-trending fracture zone that is generally spatially correlative with the chasmata. Steep scarps associated with coronae and the fracture zone impart on this region some of the most continuous steep slopes on Venus. Individual flows from the numerous coronae and from the fracture zone are cut by structures associated with either coronae or the fracture zone, or both; yet individual flows from coronae and the fracture zone also postdate such structures, indicating intimate temporal relations between tectonism and magmatism within the fracture zone as well as individual coronae.

The Nuahine Tessera material inlier (unit tN) comprises locally deformed crust that exhibits high backscatter (–9.13 to –10.30 dB). Structures include two sets of near orthogonal (north-northeast- and west-northwest-trending) ribbon structures (long, narrow, periodically spaced ridges and troughs (Hansen and Willis, 1996, 1998; Hansen and others, 2000)), broad north-northeast-trending folds or warps (wavelength ~10–20 km), broad west-northwest-trending folds or warps (wavelength ~10–25 km), and intratessera basins. Radar-dark coronae flows of Seia Corona and a composite unit from Ceres, Bona, and Miralaidji coronae (unit cSe and unit cCBM, respectively) surround and embay the inlier along its margins. We interpret the margin as a relict topographic moat, which has been filled by corona-related flows and locally uplifted during regional contraction. Topographic lows within the tessera are also internally embayed by an intratessera basin flow unit (unit itb) (for example, Banks and Hansen, 2000); embayment patterns reveal the detailed structural topography of the ribbon-fold terrain. Intratessera basin material (unit itb) commonly preserves primary shield edifices and does not exhibit tessera-related structure, and thus, at least the surface flows postdate ribbon and fold formation and therefore also postdate the material unit(s) that hosts tessera deformation fabrics. The origin of the material unit(s) that hosts the ribbon-fold fabric is unknown but presumably of volcanic origin as argued above. For a complete discussion of tessera deformation see Hansen and others (2000) and references cited therein.

Apart from Nuahine Tessera the map area is areally dominated by four major and nine minor coronae-related units, two fracture zone-related units, a unit consisting of volcanic shields, and five units that form small kipukas within the other units. Most units are variably cut by generally north- to north-northwest-trending wrinkle ridges.

The units that underlie the coronae-related units include relatively small regions exposed mostly as kipukas (basement) in the north to central (basal unit a, ba), central (basal unit e, be), south-central (basal unit d, bd), southeast (basal unit c, bc), and northeast (basal units bb1 and bb1) regions of the map area. In each case the units are preserved due to their local elevation relative to their surroundings; that is, they are preserved as kipukas. The relative age of each of these basal units is indeterminate given that they are not exposed in mutual contact and it is for this reason that we do not use a single unit name to define them.

Unit ba (prR1 of DeShon and others, 2000), the areally most extensive basal unit, is a radar-dark, smooth unit that exhibits low backscatter (–17.63 to –18.36 dB). Topographically, unit ba is preserved within broad northeast- and northwest-trending warps (DeShon and others, 2000). The outcrop pattern of unit ba preserves evidence of the north-east-trending warps that must have formed after unit ba emplacement, but before the emplacement of surrounding units. The northwest-trending warps deform both unit ba and younger surrounding units as observed in stereo and synthetic stereo imagery and supported by the map pattern. A suite of regional northeast- to east-northeast-trending extension fractures cut unit ba but does not cut overlying units, providing strong temporal constraints and further indicating a period between the emplacement of unit ba and younger surrounding units. Kipukas of unit ba are preserved across a region over 1,000 km square; similar fractures are also documented in a stratigraphically low unit up to 1,500 kilometers to the north in Rusalka Planitia quadrangle (V–25) (Young and Hansen, 2000). A sinuous, 60-km-long canali cuts unit ba near 10.5° S., 163.5° E. The canali predates the northeast-trending fractures because it is not obviously affected by the fractures, and it postdates unit ba because it appears to cut unit ba (DeShon and others, 2000). However, the canali could have formed as a lava tube in unit ba, responsible in part for the emplacement of unit ba; yet the linear topographic depression, the canali itself, may have formed due to later collapse of the lava tube, and therefore could have formed before or after the northeast-trending fractures—that is, the canali could represent a collapsed lava tube, which formed before the northeast-trending fractures and collapsed after (or during) northeast-trending fracture formation. Age relations between units tN and ba are unconstrained. These two units are not in mutual contact, and their age relation with later secondary structures are similar; thus any interpretation of relative age depends on modes of their respective formation. Given that unit tN is interpreted as having formed locally above a mantle plume as it impinged on the surface (for example, Hansen and Willis, 1998; Phillips and Hansen, 1998), unit ba could simply represent material that was contiguous with the material that hosted unit tN formation, yet was locally unaffected by the plume head. However, unit ba could be older or younger than the host of unit tN deformation.

Basal unit bb2 is the next most areally extensive unit. This region also includes kipukas of an older unit (basal unit bb1) that is locally deformed into north-northeast-trending ridges interpreted as folds (for example, Stofan and others, 1993; Keep and Hansen, 1994; Hansen and Willis, 1996). Unit bb2 embays folded unit bb1, yet is itself locally folded along parallel trends, indicating that folding began before, but continued during and after, unit bb2 emplacement. The deformed region also hosts local shields, the flows of which might also be variably involved in folding. Unit bb2 hosts distinctive arcuate fractures, commonly with "T" terminations. Timing between fold and arcuate fracture formation is unconstrained, although both, at least in part, postdate emplacement of unit bb2; folding was time transgressive, and fracturing could have been as well.

Unit bc, which comprises a single kipuka in the southeastern part of the map area, hosts fractures of several orientations, some but not all of which parallel concentric and radial fractures associated with Atahensik Corona (and therefore may be related). Unit bc is surrounded by flows, some of which are sourced from nearby Flidais Corona (unit cF) and the fracture zone to the north (unit fzcu), or from unknown sources (unit fzca). At least part of unit fzca, fracture zone and corona flow material unit a, might be sourced from the fracture zone, from nearby coronae, or from local to undefined sources. Unit fzca postdates emplacement of adjacent parts of units bc and fzcu, as these units preserve richer deformational histories. Units bc and fzca could include early flows from Atahensik Corona (unit cA).

Along the south-central boundary of the map area, unit bd hosts numerous orientations of fractures and folds and is almost surrounded by flows from Atahensik and Bona coronae. This unit could be a composite unit of various age flows, including early flows from the two coronae whose younger flows surround it. The inlier records a complex geologic history that is not explored at the scale of the current map.

Basal unit be, which lies within the Miralaidji Corona complex, hosts a penetratively developed deformation fabric variably composed of ridges, troughs, and fractures. The fabric pattern varies across the region of unit be exposure. Because the scale of the deformation is below the SAR data resolution and because the fabric lacks coherent pattern trends, we characterize this unit by its fabric—a practice which should not be undertaken lightly (Hansen, 2000). The fabric of unit be could record deformation of a unit that has no genetic relation to the corona complex it predates, or it could represent an early stage of corona complex formation. The current data resolution does not allow us to differentiate between these two interpretations.

Coronae-related lava flows dominate the map area. Coronae-related lava flows of Eigin and Saunau coronae, unit cES (prR2 of DeShon and others, 2000)), which is marked by dark to moderately bright radar return, forms the most areally extensive unit that defines a mostly contiguous map pattern locally enclosing kipukas of unit ba. The irregular contact between units ba and cES follows broad, gentle topography. Lava flows of unit cES locally fill and truncate the north-east-trending fractures that cut unit ba (for example, 10.3° S., 164.5° E.; DeShon and others, 2000). Unit cES is, in turn, uplifted along broad northwest-trending warps that parallel broad warps which preserve elongate outcrops of unit ba. These relations indicate that distal unit cES lava flows are low viscosity floodlike lava flows and that fracturing and topographic uplift of unit ba predated unit cES and continued after unit cES emplacement. Kipukas of fractured unit ba provide further evidence that unit cES postdated emplacement of unit ba. Details of the contacts between units ba and cES indicate that unit cES flows are quite thin (DeShon and others, 2000). The documented temporal sequence is also consistent with a 1° decrease in rms slope from unit cES to unit ba, if the model of progressive weathering of flows outlined in Arvidson and others (1992) is correct. Weathering rates are unknown on Venus, but if they are low (Wood, 1997), the time between emplacement of unit ba and that of unit cES may be quite large based on the difference in rms, but is unconstrained. Other contact relations with unit cES are discussed as pertinent units are introduced. Locally individual lava flows within unit cES postdate wrinkle ridge formation as evidenced by flow boundaries abutting and flowing around low topography wrinkle ridges (for example, 4° S., 168.5° E.); yet these same flows are deformed by wrinkle ridges of a similar north-northwest trend. These relations, best observed in stereo imagery, indicate that wrinkle-ridge formation is diachronous relative to unit cES emplacement, which is also diachronous. Although we extend the boundary of unit cES west to exposures of unit ba, it is possible that unit cES could end short of this contact as indicated by the dashed contact on the map. If this is the case an additional basal unit must be considered. That unit would have postdated the emplacement of unit ba, as well as the development of northeast-trending fractures and the development of northeast-trending warps of this same surface. Given the absence of clear evidence for such a basal unit and the gradational nature of unit cES, extending unit cES to the west, as we have, is the most conservative interpretation.

The northwest part of the map area is dominated by Seia Corona flow material, unit cSe, flows that extend outward from the north-northeast-trending Seia Corona complex, and an incipient corona east of Seia. These flows embay a topographic moat to the north and east of the tessera inlier. The eastern boundary of unit cSe is marked by the broad warp of uplifted unit ba, thus indicating that the north-northwest-trending warp existed, at least in part, before unit cSe emplacement. Synthetic stereo data indicate that unit cSe is uplifted along the western boundary of the warp and thus uplift likely continued after unit cSe emplacement. The contact between units cSe and cES is gradational, and relative temporal relations are unconstrained. The southwestern boundary of unit cSe is consistent with mutual embayment of unit cSe and coronae-related flows to the south. The southern and southeastern boundary of unit cSe is poorly defined. This unit may extend to the contact with units tN and itb as shown on the map, or the unit could end north of this boundary as indicated by the dotted contact (see map), in which case an additional basal unit must be considered. As discussed above, an additional basal unit might exist—such a unit would likely predate units cSe and cES, yet it must postdate the emplacement and deformation of unit ba. Given the absence of solid evidence for such a unit, we have chosen the simplest geologic relations that are consistent with the available data and extended units cSe and cES to the east and west, respectively, to their lowest topographic points and interpreted a contact relation between them. We also chose to extend unit cSe to the contact with units tN and itb in the south. Unit cSe is a composite unit of diachronous flows as indicated by detailed flow and fracture relations. Earlier flows are cut by north-northeast-trending Seia-related fractures, yet other flows cover these same fractures.

Unit cCBM, a composite unit, includes flows from composite coronae Ceres, Bona, and Miralaidji (and a small-unnamed corona (17° S., 162.5° E.)), and dominates the central and southwestern parts of the map area. This unit displays perhaps the most variable radar characteristics, ranging from radar dark to bright (–7.18 to –17.89 dB); the range in backscatter is likely a function of both flow facies and tectonic fabric facies. The lobate character of numerous flows provides strong evidence of flow sources and directions (flow arrows). Although many details of individual flows are apparent at 1:5 million scale SAR, the boundaries between flows are indeterminate across the map area even at the highest resolution data. Indeed the variability of radar brightness, which serves to show flow directions and lobate character, may be due to changes in flow roughness within single flows and need not indicate distinct flows. Additionally, distinctly different flows may have the same radar brightness. At the larger scale, boundaries between flows sourced from the three major and one minor coronae are indeterminate, which is why we combine these flows into a single map unit. We distinguish four subunits locally—a particular lobate unit within Miralaidji (cMa) and three radar dark units (~–13.95 to –16.02 dB) within the interior regions of the three major coronae, units cCa, cBa, and cMb within the central regions of Ceres, Bona, and Miralaidji coronae, respectively. Each of these units formed relatively late with respect to formation of radial or concentric fracturing of their respective coronae. These units almost certainly result as a continuation of earlier formed flows, and the radar dark and relatively undeformed surface simply represents a final phase of interior corona volcanic processes. We also delineate Miralaidji Corona unit a, cMa, within Miralaidji Corona. Unit cMa displays lobate to digitate flows having a wide range in radar brightness (–11.59 to –20.00 dB). These flows emanate from radial or concentric fractures related to Miralaidji Corona formation; locally radial or concentric fractures cut the flows. Although we delineate the boundaries of this unit on the lobate character of the flows, individual flow units actually may extend locally beyond the moderately sharp lobate boundaries (and start interior of unit cMa). In some places the lobate character of the flow front is poorly defined at highest SAR resolution, yet it appears more clearly defined at lower data resolution. Flow line data within units cMa and cCBM reflect topographic gradients during flow emplacement and thus provide relative temporal relations between flow emplacement and chasmata formation. Locally flow indicators suggest that individual (?) flows traveled great distances, perhaps greater than 700 km in some cases. In the case of Ceres and Miralaidji coronae, flows sourced from the corona interiors extend across associated chasmata, thus indicating that chasmata (topographic trough) formation dominantly postdated emplacement of these corona-sourced flows. Locally some flows spill into the chasmata, which indicates limited flow activity after chasmata formation. Along its northern boundary unit cCBM flows are directed outward from the Ceres and Miralaidji complexes. In the central part of the map area unit cCBM flows enclose local upwarps of unit ba. Contact relations between cES and cSe do not allow us to determine relative timing between these composite units and composite unit cCBM. Given that each unit comprises numerous (individual) flows, temporal relations may well be broadly synchronous due to the diachronous nature of flows that compose each composite unit. Thus, even if we were able to robustly constrain relative temporal relations along the boundaries of these units (which we are not able to do), we would not feel comfortable extrapolating local temporal relations to the whole of the units. Both units are similarly temporally confined with regard to unit ba and uplift. North of Diana Chasma and north of the Miralaidji Corona complex, unit cCBM locally embays the tessera inlier (unit tN), and flow lines indicate that at least at one time a topographic trough or moat bounded the southern margin of tessera, which focused flows along this boundary. In the west-central part of the map area unit cCBM flows spill through and around tessera kipukas. The northwest boundary of unit cCBM with unit cSe shows broadly synchronous relations between these composite flow units. The detailed spatial and temporal preservation of flows and fractures indicate that corona volcanism and tectonism were broadly coeval across individual coronae and that coronae record rich volcanic and tectonic histories as documented by others (for example, Chapman 1999; Chapman and Zimbleman 1998; Copp and others, 1998)

Flows from Atahensik Corona (unit cA), the largest corona in the map area, dominate the south-central region. Unit cA, like other corona-flow units, compises numerous flows sourced from the central region of Atahensik Corona, or from associated concentric or radial fractures (back scatter –13.95 to –16.98 dB). Evidence of flow direction is preserved locally within the corona interior and extensive flow lines, and fronts are preserved in the western part of unit cA. The western and southeastern boundaries of unit cA are perhaps the best defined, whereas the eastern and northern limits are gradational and difficult to define due to intensive fracture formation as well as similarity in overall radar characteristics of adjacent units. The easternmost boundary shows detailed diachronous (?) interaction with radar bright fracture zone sourced flows (unit fz). Although temporal relations are difficult to constrain, unit cA flows apparently predated unit fz. Unit fz flows are predominantly preserved in the southeastern part of the map area. Also at this location Henwen Fluctus flows, unit fH, comprise radar bright and radar dark flows (–9.88 to –14.06 dB) that emanate from local fracture zone structures. The radar bright and dark flows together preserve a record of lobate flow fronts, levees, breached levees, well preserved flow direction indicators, and local channels. We have delineated radar bright and dark facies within this unit by black lines. The bright and dark radar patterns are consistent with broadly synchronous flow facies of variable roughness. The reader is encouraged to examine the radar data for detailed flow patterns and data. Within this region flow directions are consistently to the south and provide a clear record of paleoslope. Steep east-northeast-trending scarps, presumably related to normal faults, cut the flows, thus dropping the source or proximal flows from the distal flows. This relation indicates that scarp formation postdated the emplacement of these flows. Locally within the fracture zone, radar bright flows parallel and follow trough valleys, which indicates that some of these flows postdate local trough formation. Locally these flows also appear to follow a paleotrough along the eastern margin of Atahensik Corona, yet Atahensik Corona-related radial fractures and concentric folds, fractures, and scarps also locally cut the flows. These relations indicate that unit fz flows are broadly synchronous with the (extended) evolution of Atahensik Corona and with the extended evolution of the fracture zone. Unit fH flows are also broadly synchronous with fracture zone evolution, although these localized flows were emplaced relatively late during the evolution of the fracture zone as evidenced by the locally coherent nature of the flows (that is, unfractured).

The six relatively small corona flow materials, units cF, ca, cb, cSi, cK, and cN, exposed from south to north, respectively, within the eastern part of the map area, are each sourced from individual coronae interiors. Flidais Corona flow material (unit cF) comprises radar dark to bright lobate flows (–15.88 to –17.38 dB) that spill outward from Flidais interior. South of the map area these flows extend for great distances (perhaps greater than 2,000 km) into Zhibek Planitia. Contact relations between units cA and cF indicate that unit cF is generally younger, although local evidence for the opposite temporal relations exist. (Again, these two coronae likely formed in a broad synchronous fashion.) Flow indicators within unit cF parallel the contact between units cF and fzcu and indicate that unit cF was emplaced, at least in part, after emplacement of at least some individual unit fzcu flows. In addition, unit fH flow indicators parallel the unit cF contact, indicating that unit fH, at least in part, postdated the emplacement of unit cF. Unit cF flowed around and locally through units bc (southeastern basal unit) and fzca, a kipuka of stratigraphically lower material that could have been surfaced by earlier flows from Atahensik Corona (for example, unit cA) or that could represent a locally preserved outcrop of pre-cA material. Unit bc preserved suites of fractures (likely composite) that are not preserved together elsewhere. Some of the fractures possibly formed as radial and concentric to Atahensik Corona. Northeast-trending fractures preserved in unit bc are similar in trend and character to fractures that locally cut unit fz to the north.

Unit cF is locally overlain by flows from an unnamed corona that resides in V–38 quadrangle to the east (unit ca). (Along the easternmost boundary of the map area at ~20° S., flows from another unnamed corona in V–38 quadrangle, unit cb, barely spill into the map area.) Although contact relations indicate that unit ca generally overlies and thus postdates unit cF, fractures radial to Flidais Corona and interpreted as recording a part of that corona formation cut unit ca flows, thus indicating that Flidais flows (unit cF) dominantly predate formation of Flidais' preserved radial fractures. Such relations provide evidence of stages in Flidais Corona evolution. That is, unit ca was emplaced dominantly after corona flows of unit cF but before radial fracturing associated with Flidais Corona formation.

Similar temporal relations and evolutionary history are preserved at Sith Corona and Khabuchi Corona, west of Sith. Preserved Sith Corona flows (–10.10 to –12.34 dB), unit cSi, flowed outward and are best preserved to the north. To the south the flows are disrupted by secondary fracture zone structures. Flows from adjacent Khabuchi Corona (unit cK; –11.76 to –13.69 dB) spill over unit cSi near the center of Sith and to the north, which indicates that this corona is generally younger than Sith, a relation consistent with the relative topography of these adjacent coronae. However, along the southern flanks of these coronae temporal relations between units cSi and cK are less clear. Flows included with unit cSi emanate from fractures associated with the fracture zone, rather than with Sith Corona. Also, the two coronae likely have intermingled flows. Fractures radial to and concentric to Sith Corona are locally filled by unit cSi and cut units cSi and cK, indicating that such fracturing is diachronous and that fracture formation extended, at least in part, to relatively late in the evolution of Sith Corona. The northern boundary of unit cSi is gradational with unit cES flows. In contrast, contact relations of units cK and cES indicate that unit cK dominantly postdates the parts of unit cES along their contact. However, temporal relations derived along this single contact cannot be robustly extrapolated to all of unit cES, clearly a composite unit. To the south unit cK flows into the fracture zone and covers preexisting fractures, yet they are also cut by younger fractures, which indicates broadly synchronous formation. Contact relations between unit cK and flows from Miralaidji Corona (included in unit cCBM) show mutual embayment, indicating overlapping temporal relations.

Nirmali Corona flow material (unit cN) exhibits clear flow direction indicators and lobate flow fronts (–11.36 to –13.12 dB). Whether this unit represents the entirety of flows from Nirmali Corona or simply the radar distinct flows of a corona having larger areal extent is not clear. Flow directions in the adjacent part of unit cES, which generally surrounds unit cN, are consistent with a source from Nirmali Corona, but some are also consistent with an Eigin Corona source, or an incipient corona source.

The east-central part of the map area is dominated by fracture zone and corona flows, undivided (unit fzcu), which probably include basal flows (?), flows sourced from fracture zone fractures, and some corona-derived flows (some coronae are in V–38 quadrangle; backscatter –8.91 to –14.60 dB). Locally preserved flow fronts provide evidence of flow direction, but division of this unit is greatly hampered by the intense character of fractures and steep scarps associated with the fracture zone. The eastern part of this unit may be sourced, at least in part, from the large Zemina Corona complex as well as from an unnamed incipient corona to the east. The northernmost part of unit fzcu exhibits flow indicators that show flow from the south-southeast, yet also displays the arcuate fractures that deform unit bb2. The contact with unit bb2 is interpreted as a thinning of distal flows that allows incomplete covering of the underlying curved or arcuate fractures (shown as dashed contact). We define the limit of unit fzcu as the boundary between clearly defined arcuate fractures in unit bb2 and present, but less clearly demarked, arcuate fractures, interpreted as fractures covered by unit fzcu flows. Although we could have defined the limit of unit fzcu as the "disappearance" of arcuate fractures to the south—interpreted as fractures covered within thicker flows of unit fzcu—we define the contact as the limit of unit fzcu, reasoning that if fractures are even thinly covered the covering unit is present. The contact of unit fzcu with unit cES does not provide consistent robust temporal relations, and we interpret that these composite units broadly overlap temporally. Any temporal relations that could be demonstrated for unit fzcu could not be extrapolated to the entire unit because this unit is a composite unit as mapped, as is unit cES. The scale of the map relative to the scale of flows and structural complexity does not allow robust spatial or relative temporal division.

Shield field flow material (unit sf) exhibits relatively high radar backscatter (–13.10 to –13.88 dB) and a mottled texture marked by circular bright patches; unit sf hosts abundant shields. Unit sf cannot be distinguished from unit cES on the basis of topographic or surface roughness differences, and these units may be gradational. The paucity of sharp circular contacts associated with individual shields may provide evidence that the shields and their flows generally lie stratigraphically above unit cES, although the two composite units could have, in part, temporally overlapped. If unit cES dominantly postdated emplacement of unit sf and if unit cES flows had flowed around local topographic highs formed by individual shields, we might expect sharp circular contact to be preserved—such relations are rare, though preserved locally. Radar differences between the two units may have degraded with time (for example, Arvidson and others, 1992). Numerous shields are preserved within unit cES as shown on the map. This relation could be supportive of general synchroneity, but need not be. In fact shields are geomorphic features, primary structures that likely reflect, at least in part, petrology, viscosity, and fluid content of parent magma—characteristics which may or may not exhibit regional or global temporal significance. Although we delineate units sf and cES as two different units, they may well represent different volcanic facies of the same unit.

Detailed mapping within the chasmata is hampered in part by severe layover; however, local patches of radar brightness along the slopes of chasmata are interpreted as landslide or mass wasting deposits (unit ls; –8.10 to –14.45 dB). The regions are narrow up-slope and broaden down-slope with lobate margins; patches of radar darkness up-slope from the deposits are interpreted to be breakaway zones.

The map area also hosts two isolated volcanic edifices, including a 30-km-diameter steep-sided dome (150.8° E., 2.9° S.; Pavri and others, 1992) and a shield having a summit diameter of ~10 km (152.3° E., 9.9° S.).

TECTONIC STRUCTURES

The map area contains a range of tectonic or secondary structures associated with tessera terrain, regional fracture suites, wrinkle ridges, minor fold belts, fracture zone structures, and coronae-related structures. The chasmata, coronae, and fracture zone structures are locally spatially separate from one another, yet they also locally spatially overlap. For example, the chasmata define the circular troughs of large coronae, and the fracture zone displays more intense, or more closely spaced, fractures within the steepest part of some chasmata. These overlapping spatial relations may indicate gross genetic relations between and among some coronae, chasmata, and parts of the fracture zone. We describe each suite of structures briefly below in the order presented above.

TESSERA DEFORMATION

Nuahine Tessera preserves ribbon structures (Hansen and Willis, 1996, 1998) and folds. Within the Nuahine Tessera inlier, ribbon wavelength, marked by ribbon ridge width (<2.5 km), indicates a shallow depth to the brittle ductile transition (BDT) at the time of ribbon formation (Hansen and Willis, 1998), whereas the greater fold wavelength reflects a depth to the BDT of ~6 km (Brown and Grimm, 1997), consistent with documented structural relations at eastern Ovda Regio (Ghent and Hansen, 1999). Given the spatial association of ribbons and folds, it is most mechanically reasonable that ribbon structures broadly predate fold formation (Hansen and Willis, 1998; Hansen and others, 2000), as supported by detailed mapping in eastern Tellus Tessera (Banks and Hansen, 2000). The similarity of the ridge spacing for both ribbon suites reflects a similar layer thickness, indicating that the two ribbon suites likely formed broadly synchronously. Temporal relations between the two fold suites are similarly unconstrained. As stated above, age relations between the material which hosts the ribbon structures (unit tN) and nearby basal flow unit ba are unconstrained. These two units are not in mutual contact; thus any interpretation of relative age depends on modes of their respective formation. Given that unit tN is interpreted as having formed locally above a mantle plume as it impinged on the surface, unit ba could simply represent material that was contiguous with the material that hosted unit tN formation, yet was locally unaffected by the plume head. However, unit ba could be older or younger than the host of unit tN deformation. Similarly the relative timing of ribbon and fold formation, structures preserved in unit tN, and the timing of the emplacement of unit ba is unconstrained.

REGIONAL DEFORMATION

Northeast-trending extension fractures that cut unit ba help define temporal relations between unit ba and surrounding units (assuming that the fractures formed over a relatively distinct time interval) (DeShon and others, 2000). The northeast-trending fracture set consists of one to five radar-bright lineaments per fracture; wider fractures in the south appear to have two to four terraces defining each edge. The open fractures have topographically raised edges, giving the fracture a distinctive double-lipped appearance. Fracture characteristics include spacing of 1 to 10 km, lengths from 10 to 100 km, and widths that grade from 1 to 1.5 km in the south to 0.1 to 1 km in the north. Along the contact between units ba and cES northeast-trending fractures in unit cES are relatively poorly defined and radar dark compared to parallel fractures that cut unit ba. The similar spacing and trend of these fractures is consistent with the interpretation that they represent a single, genetically related fracture set even though fracture appearance changes somewhat across ~1,000 km perpendicular to the fracture trend. In the north, the northeast-trending fractures appear to thin and to lose the wide, multiple-edged appearance. The northeast- to east-trending fractures that cut unit bc may be similar to these fractures, but it is impossible to be sure given that the region between units ba and bc are covered by a host of younger units. For a more complete discussion of fractures, units, and topography refer to DeShon and others (2000).

A distinctive pattern of arcuate fractures cut unit bb2 in the northeast corner of the map area. The fractures trend variably northeast, northwest, north, and east. Straight to arcuate traces and "T" terminations distinguish these fractures from other fractures in the map area. Along the southern contact of units bb2 and fzcu the arcuate fractures become less well defined. We interpret that this is due to local filling of fractures by unit fzcu. The fractures end more abruptly along the unit bb2—cES contact to the west, although locally the fractures are traceable into unit cES. We interpret these relations to indicate that unit cES postdated arcuate fracture formation and that locally the distal flows of unit cES are thin enough to only locally bury the underlying arcuate fractures. The mechanism that led to the formation of these arcuate fractures is unknown. The lack of polygonal character argues against their formation as cooling fractures; similarly their lack of parallel or radial patterns distinguish them from other fracture suites.

North-northwest-trending wrinkle ridges, spaced ~5–30 km, which deform essentially all the units within the map area, are part of a broadly circum-Aphrodite Terra corona wrinkle ridge system described by Bilotti and Suppe (1999). Within the Diana Chasma region, wrinkle ridges are parallel and closely spaced in the southeast. The wrinkle ridges parallel the trend of the Class I ridge belt (Vetsorgo Dorsum) within Rusalka Planitia, outlined by prominent, closely spaced wrinkle ridges. Local evidence supports the pooling of some unit cES lava flows along wrinkle ridges, however, parallel wrinkle ridges also disrupt these flows. Thus wrinkle ridge formation was diachronous relative to the emplacement of unit cES. Determining when wrinkle ridge formation began is not possible, but the map relations and detailed flow-wrinkle ridge relations are consistent with wrinkle ridge formation over an extended period of time. The parallelism of wrinkle ridges with the chain of coronae in the northeastern part of the map area, with the Class I ridge belt, and with parallel warps taken together with the continued history of uplift of these warps (DeShon and others, 2000) provides strong evidence that wrinkle ridge formation may be diachronous over the time scale of the units preserved in the map area. Currently, Venus does not allow robust absolute age constraints on unit formation (see Hauck and others, 1998; Campbell, 1999), or on tectonism, which is even more difficult to determine (Hansen, 2000). Although the crater material (unit cu) and landslide deposits do not show obvious wrinkle ridge structures, one cannot robustly extrapolate this to temporal constraints. The landslide deposits lie within the deepest part of the chasmata and thus would not be expected to record wrinkle ridge formation. In addition, both the landslide deposits and unit cu are generally radar bright, as are the wrinkle ridges; therefore, these units provide a poor slate upon which to record wrinkle ridge formation.

North of ~7° S., 162° E. wrinkle ridges define a polygonal pattern with north-northwest- and east-northeast- to northeast trends. Northeast-trending wrinkle ridges are parallel to and coincident with earlier formed and filled northeast-trending extension fractures. Northeast-trending wrinkle ridges are also straighter and shorter (5–10 km as opposed to 45–60 km) than northwest-trending wrinkle ridges. The orientation and characteristics of northeast-trending wrinkle ridges implies structural inversion of previously filled northeast-trending fractures (DeShon and others, 2000).

In the southern part of the map area wrinkle ridges trend broadly north, consistent with wrinkle ridge trends in Zhibek Planitia (Bilotti and Suppe, 1999). Fold belts associated with Bona and Atahensik coronae and with the Miralaidji corona complex typically parallel the trend of local wrinkle ridges, which describe broad generally northerly trends that bend around their respective coronae complexes. Fold belts and fold height, width, sinuosity, and wavelength differentiate wrinkle ridges; locally they grade into one another such as on the western margin of Bona Corona.

These coronae-related fold belts differ from the fold belt preserved in the northeast corner of the map area in their association with coronae. The northeast fold belt hosts north-trending folds that were clearly active over an extended timeframe relative to surface flows and resulted in exposure of unit bb1. Detailed geologic relations indicate intimate relations between flow formation and uplift, similar to the detailed history documented for ridge belts in the Baltis Vallis region of V–13 quadrangle (Stewart and Head, 2000). Various levels of terraces are preserved along the fold belt margins, and the folds variably deform flows. This fold belt, which also is host to numerous shields, parallels a more extensive fold belt along strike in V–25 quadrangle. Adjacent northwest-trending wrinkle ridges trend at a relatively high angle to the fold crests within the fold belt, although immediately adjacent to the fold belt wrinkle ridges trend parallel to the fold belt folds (north-northeast). Thus fold belt formation likely began before wrinkle ridge formation, although uplift probably continued during wrinkle ridge formation. Detailed relations indicate that the fold belt represents a mechanical anisotropy that has affected later strain partitioning. The relations described briefly here are not illustrated in the map due to scale restrictions.

Diana and Dali chasmata, two of Venus's deepest chasmata, display slopes >30 degrees (Ford and Pettengill, 1992). Large-scale east-west fractures follow the topography of the chasmata but cannot alone mechanically account for the great depth of the chasmata. The chasmata represent neither rift zones of great crustal extension nor subduction zones nor regions of crustal recycling (Hansen and Phillips, 1993). Chasmata may represent the spatial correlation and interaction of coronae formation processes and fracture zone formation processes (Hansen and others, 1997; Stofan and others, 1997). Local down-dropping of the crust along the length of the chasma might be explained by finite element/finite difference modeling of large-scale corona formation by thermal diapirs (Smrekar and Stofan, 1997).

A ~300-km-wide northeast-trending fracture zone extends into the map area and crosscuts most features in its path (fig. 1*B*). Fractures and faults are predominately parallel, spaced ~1 to 15 km, and vary from ~25 to 150 km in length. The zone partitions strain along the northern and southern boundaries of Atahensik, Miralaidji, and Ceres coronae and continues along strike past the coronae extending outside the map area. Lava flows associated with faults and fractures locally constrain the relative age of deformation. Steep fault scarps parallel the fracture zone and fracture zone structures. Faults down-drop blocks of material along the east-central margin of the map area and form local topographic highs. Within this region, the fault blocks generally step downward from the south to the center of the fracture zone, although locally opposite stepping is preserved. From the central region northward the trend of the fracture zone and the stepping relations are less consistent. To the west fracture zone strain is partitioned around the major coronae, including Atahensik, Miralaidji (complex), and Ceres (complex), resulting in generally more localized strain and steeper chasmata slopes (for example, Dali Chasma along the northern and southern annuli of Atahensik and Miralaidji, respectively, and Diana Chasma along the northern and southern annuli of Miralaidji and Ceres, respectively). Fracture zone structures become more diffuse and regionally developed west of Dali Chasma. In general, fracture zone formation occurred synchronous with or after coronae formation—that is, the topographic signature associated with fracture zone formation evolved broadly synchronously with the latest stages of coronae evolution.

DEFORMATION RELATED TO CORONAE FORMATION

Five suites of structures are spatially, and thus genetically, related to coronae: linear folds or ridges, concentric folds or ridges, radial fractures, concentric fractures, and straight to arcuate normal fault scarps. An individual corona may host some or all of these structures, and in most cases these structures evolved in intimate spatial and temporal relation with corona-associated flows. The relative timing of these structures to one another and to flows of individual coronae seems to be corona specific. For example, radial fractures within Miralaidji Corona predate flows as they are locally filled with radar dark flows, whereas radial fractures of Athensik Corona show little filling by late lava flows in the corona interior. Similarly concentric fractures are locally cut by flows, and also cut flows.

Coronae Ceres, Miralaidji, and Atahensik, the largest coronae, host both radial and concentric fractures. Miralaidji shows early radial fractures and associated low-viscosity lava flows that fill an early-formed concentric topographic moat. An inner suite of concentric fractures predates an outer suite based on crosscutting relations of related lava flows, which escaped from the fracture suites. Fracture patterns of Ceres and Atahensik Coronae are not as perfectly radial or concentric as those of Miralaidji Corona (comprising the eastern part of the Miralaidji complex). Radial fractures commonly provide an avenue for flows whether the flows are observable at the surface along the length of the fracture or can be seen emanating from more distal parts of the fracture (as is the case for Atahensik and corona a). Ceres and Atahensik coronae, and the central and western part of the Miralaidji Corona complex, are bounded by deep, fractured chasmata rather than lava-filled moats. Flow indicators taken together with fracture and topography patterns indicate that radial flows from each of these regions extended spatially beyond the present limits of the chasmata, and predated chasmata formation. As previously noted (Hansen and Phillips, 1993), in the case of Atahensik Corona, radial fractures also extend well beyond the chasmata, an observation inconsistent with proposed subduction zone interpretations (McKenzie and others, 1992; Sandwell and Schubert, 1992a, b). Map relations are consistent with relatively late formation of the chasmata and agree with temporal relations outlined by Squyres and others (1992), and genetic association of chasmata and coronae (Stofan and others, 1997).

The topographically high centers of these coronae are elongate along an east-west axis, with fracture sets that favor east-west trends consistent with formation within a regional strain field characterized by north-trending principal elongation. Seia Corona shows concentric fractures and north-northeast-trending fractures, consistent with regional west to northwest elongation. In the northeastern part of the map area concentric ridges and northwest-trending wrinkle ridges or folds mark a northwest-trending chain of small coronae. South of Aphrodite Terra, Bona Corona to the west and Flidais Corona to the east each display radial and concentric fractures. Bona Corona is also spatially associated with concentric ridges and with a small ridge belt that may be genetically related to corona formation.

Two main fold belts trend generally north-south. The west fold belt (16.5° S., 156.5° E.) marks the western edge of the Miralaidji Corona complex. Along its southern boundary the ridge belt refracts around Dali Chasma. The lack of clear truncating structures of the fold belts by the chasmata indicates that the two structures may have formed broadly synchronously. Another fold belt (22° S., 175° E.) resides within the southeast margin of Atahensik Corona; the fold complex does not wrap around the northern and southern boundaries of the corona nor is it developed along the western margin. Northeast of Atahensik Corona the fold belt tracts into the fracture zone; it is preserved locally in regions of low fracture density, suggesting that the folds probably broadly predate many of the fractures. Similarly, flows of unit fz flood into the troughs of local folds and are locally uplifted along these structures. These relations indicate that Atahensik evolution likely overlapped in time with the evolution of the fracture zone.

Small fold belts related to Bona Corona and to several small coronae in the northwest-trending corona field form semi-concentrically around the central depressions. Northwest-trending ridges and folds, rather than fractures, dominate the northwest-trending corona field. These trends are consistent with corona formation within a bulk strain field having northwest maximum elongation.

IMPACT CRATERS

Diana Chasma quadrangle hosts up to 17 impact craters ranging from 2.5–71.8 km in diameter and four shock features (table 1). Ejecta blanket materials, impact structures (that is, rim, central peak, and so on), and flow material (that is, impact melt, fluidized ejecta, or subsurface magma) are undifferentiated for all craters (excluding Markham and Langtry) and mapped as undifferentiated crater material (unit cu). Seven craters (Alison, Dheepa, Langtry, Markham, Martinez, Warren, and Zeinab) exhibit complete or partial interior flood lava (dark floors), indicating that these craters are likely older than the bright-floored craters (Izenburg and others, 1994). Herrick and others (1997) discuss possible volcanic sources for and the implications of interior flooding. Warren, Martinez, Gulnara, and Langtry display interior fractures related to local deformation processes. Alison, Blanche, and Patimat are associated with small dark semi-degraded parabolas. Patimat crater exhibits wind-blown ejecta material that forms a diffuse, radar bright layer to its west. Blanche and Markham are associated with far-field ejecta flows in addition to ejecta blankets; Dheepa ejecta locally follows preexisting fractures, implying flow (and temporal relations), but it does not exhibit a far-field ejecta flow.

Markham, a 71.8-km-diameter crater within Rusalka Planitia, is associated with an extensive far-field outflow, Markham crater flow material (unit cfM), and a small ejecta blanket—Markham crater impact materials (unit ciM). The ejecta blanket appears stippled on SAR, indicating the material may be blocky and incoherent. The sector of missing ejecta in the southwest, the shape of the rim, the offset peak, and the ejecta shape indicate that this crater resulted from an impact angle of 10°–20° (Schultz, 1992). The outflow appears very bright on SAR imagery and extends to the east, following present-day topography. Locally, the outflow interacts with preexisting fractures, filling and following northeast fracture trends. Wrinkle ridges buttress the outflow along the eastern margin, though the outflow unit covers small ridges near its source. Flow patterns within the outflow unit appear ropy. Kipukas of underlying material indicate that the flow was interacting with small variations in local topography, and therefore we suggest that flow viscosity was very low during emplacement. The outflow is likely enhanced due to the crater's location adjacent to a small corona.

GEOLOGIC HISTORY

Diana Chasma quadrangle records a broad geologic history of early local tessera formation followed by coronae, chasmata, and fracture zone formation. Tessera ribbon formation records local extension of previously formed flow(?) material with a local shallow BDT; tessera fold formation reflects minor contraction with an increased depth to local BDT. Intratessera basin lava locally embays ribbon troughs and fold valley. These lava flows sit topographically high relative to the embaying flows from surrounding coronae and thus likely formed late during the formation of the tessera tectonic fabric (for example, Banks and Hansen, 2000). Coronae, chasmata, fold belt, and fracture zone formation require a relatively deep BDT (Hansen and others, 2000).

Geologic mapping of the lava flows and secondary structures in southern Rusalka Planitia reveal a geologic history recording the complex interactions of volcanism, tectonism, and topography. Southern Rusalka Planitia units record tectonic and volcanic history. Unit ba hosts northeast-trending extension fractures that widen to the south. Unit ba was locally uplifted along northeast-trending arches before unit cES emplacement and was uplifted along northwest-trending arches before or synchronous with unit cES emplacement. Low viscosity lava flows of unit cES, the most areally extensive unit in the map area, includes a conglomeration of multiple, thin lava flows (DeShon and others, 2000); these lava flows fill local topographic lows and northeast-trending fractures. Unit cES is similarly locally uplifted along northwest-trending arches, which indicates that topography continued to evolve during and after unit cES emplacement. Unit sf is probably intimately related to unit cES. Temporal relations between these two composite units are indeterminate, possibly indicating broadly coeval evolution.

The chain of coronae extending along the northeastern part of the map area displays a dominance of northwest-trending ridges rather than fractures, and as such they record a bulk strain regime having a northeast-trending axis of maximum shortening (northwest-trending axis of maximum elongation), suggesting that these coronae formed within a bulk strain regime consistent with regional wrinkle ridge formation. In the western part of the map area, Seia Corona hosts dominantly northeast-trending fractures, consistent with this same regional bulk strain regime.

Central Ceres, Bona, Miralaidji, and Atahensik coronae preserve penetratively developed radial fractures and locally developed concentric fractures associated with corona formation. Chasmata define the edges of Ceres and Atahensik coronae as well as the southern and northern part of the Miralaidji Corona complex. To the north and northeast, Miralaidji is topographically defined by lava flow-filled moat rather than by a chasma. Although the fracture zone influences Ceres and Atahensik coronae more than Miralaidji or Bona coronae, fracture intensity is likely the result of location rather than relative time of formation. Any temporal interpretation must consider possible strain partitioning, and therefore interpretations are not unique. These four coronae formed broadly synchronously at the scale of the map.

Flidais Corona forms part of a coronae cluster south of the map area. Radial and concentric fractures indicate that some local processes or bulk strain or both may be influencing coronae formation in the southern region of the quadrangle.

Coronae structures—including associated fractures and fold belts, chasmata, fracture zone, and wrinkle ridges—are all consistent with a bulk strain regime having northwest-trending maximum elongation. Tessera deformation describes a more localized bulk strain regime. Diana and Dali chasmata represent the spatial overlap of the east-northeast-trending fracture zone and the similarly oriented portions of the annuli of the large coronae, Atahensik, Ceres, and the Miralaidji Corona complex. The fold belts that coincide with north-trending portions of the corona annuli reflect a similar bulk strain regime. Thus we interpret that the coronae, chasmata, and fracture zone could have formed within the same bulk strain regime as part of a large equatorial system extending beyond the map area, possibly a circum-Aphrodite Terra strain pattern recorded by regional wrinkle ridges described by Bilotti and Suppe (1999). In this region contractional structures—wrinkle ridges and folds or fold belts—are broadly parallel to one another, and extensional structures are broadly perpendicular to these contractional structures, consistent with an interpretation of time transgressive accumulation of strain within a consistent bulk strain regime.

Individual corona formation (both magmatic and tectonic) appears to be a continuing process, and lava flows may consist of thin individual flows (<1 km). These thin flows spill out into the plains topographic basin and may be responsible for much (most?) of plains resurfacing. The thin character of the flows implies that estimates of plains lava volumes and emplacement rates based on thicker lava flows (Head and Coffin, 1997) are too high (DeShon and others, 2000). Our study supports the views of planitiae evolution as discrete volcanic and tectonic processes temporally at local and regional, but not at global, scales (for example, Guest and Stofan, 1999). Mapping within Diana Chasma quadrangle is inconsistent with global stratigraphy models (for example, Basilevsky and Head, 1998, 2000; Head and Basilevsky, 1998), and the local geologic and structural relations discussed herein should not be confused with global units.

Our mapping suggests that coronae may play a critical role in Venus resurfacing and plains volcanism. Geologic relations indicate that more than ninety percent of the map area (not including tessera terrain or crater material) could be related to corona formation. Southern Rusalka Planitia is resurfaced by flows from the complex of moderate to small coronae to the east, flows from Seia Corona to the west, and flows from Miralaidji corona complex to the south. Miralaidji Corona, described as hosting moderate associated volcanism (Stofan and others, 1992), spawns flows that extend up to 750 km from the corona center. Kipuka of preexisting flows (identifiable by distinct and locally flooded north-east-trending fractures that cut the kipuka but not the overlying units) are preserved locally in broad warps; coronae flows are locally uplifted along the same or parallel warps, indicating that topography evolved throughout the geologic history of the map area (DeShon and others, 2000). Atahensik Corona, classified as deficient in associated volcanism in a reconnaissance study (Stofan and others, 1992), has produced lava flows that extend over 750 km beyond its annulus diameter in one direction; minimum estimates indicate that this single corona resurfaced over 1.4 million square kilometers, and probably a much greater area. Flows from Atahensik and Flidais coronae spill south to Zhibek Planitia and may be responsible for many of the exposed flows. Thus planitiae volcanism and coronae may, at least in part, be genetically related.

REFERENCES CITED

Arvidson, R.E., Greeley, R., Malin, M.C., Saunders, R.S., Izenberg, N., Plaut, J.J., Stofan, E.R., and Shepard, M.K., 1992, Surface modification of Venus as inferred from Magellan observations of plains: Journal of Geophysical Research, v. 97, no. E8, p. 13,303–13,318.
Banerdt, W.B., McGill, G.E., and Zuber, M.T., 1997, Plains tectonics on Venus, *in* Bougher, S.W., Hunten, D.M., and Phillips, R.J., eds., Venus II: Geology, geophysics, atmosphere, and solar wind environment: Tucson, University of Arizona Press, p. 901.
Banks, B.K., and Hansen, V.L., 2000, Relative timing of crustal plateau magmatism and tectonism at Tellus Regio, Venus: Journal of Geophysical Research, v. 105, p. 17,655–17,667.
Basilevsky, A.T., and Head, J.W., 2000, Geologic units on Venus: Evidence for their global correlation: Planetary Space Science, v. 48, p. 75–111.
———1998, The geologic history of Venus: A stratigraphic view: Journal of Geophysical Research, v. 103, no. E4, p. 8531–8544.
Bilotti, F., and Suppe, J., 1999, The global distribution of wrinkle ridges on Venus: Icarus, v. 139, p. 137–157.
Brown, C.D., and Grimm, R.E., 1997, Tessera deformation and the contemporaneous thermal state of the plateau highlands, Venus: Earth and Planetary Science Letters, v. 147, p. 1–10.
Campbell, B.A., 1999, Surface formation rates and impact crater densities on Venus: Journal of Geophysical Research, v. 104, p. 21,951–21,955.
Chapman, M.G., 1999, Geologic/geomorphic map of the Galindo quadrangle (V-40), Venus: U.S. Geological Survey Geologic Investigations Series I–2613, 1:5,000,000 scale.
Chapman, M.G., and Zimbelman, J.R., 1998, Corona associations and their implications for Venus: Icarus, v. 132, p. 344–361.
Copp, D.L., Guest, J.E., and Stofan, E.R., 1998, New insights into corona evolution: Mapping on Venus: Journal of Geophysical Research, v. 103, p. 19,401–19,418.
DeShon, H.R., Young, D.A., and Hansen, V.L., 2000, Evidence for thin plains lava flows in southern Rusalka Planitia, Venus: Journal of Geophysical Research, v. 105, p. 6983–6995.
Ford, J.P., Plaut, J.J., Weitz, C.M., Farr, T.G., Senske, D.A., Stofan, E.R., Michaels, G., and Parker, T.J., 1993, Guide to Magellan image interpretation: Jet Propulsion Laboratory Publication 93–24, p.148.
Ford, P.G., and Pettengill, G.H., 1992, Venus topography and kilometer-scale slopes: Journal of Geophysical Research, v. 97, no. E8, p. 13,103–13,114.
Ghent, R.R., and Hansen, V.L., 1999, Structural and kinematic analysis of eastern Ovda Regio, Venus: Implications for crustal plateau formation: Icarus, v. 139, p. 116–136.
Guest, J.E., and Stofan, E.R., 1999, A new view of the stratigraphic history of Venus: Icarus, v. 139, p. 55–66.
Hansen, V.L., 2000, Geologic mapping of tectonic planets: Earth and Planetary Science Letters, v. 176, p. 527–542.
Hansen, V.L., Banks, B.K., and Ghent, R.R., 1999, Tessera terrain and crustal plateaus, Venus: Geology, v. 27, p. 1071–1074.
Hansen, V.L., and Phillips, R.J., 1993, Tectonics and volcanism of eastern Aphrodite Terra, Venus: No subduction, no spreading: Science, v. 260, p. 526–530.
Hansen, V.L., Phillips, R.J., Willis, J.J., and Ghent, R.R., 2000, Structures in tessera terrain, Venus: Issues and answers: Journal of Geophysical Research, v. 105, p. 4135–4152.
Hansen, V.L., and Willis, J.J., 1996, Structural analysis of a sampling of tesserae: Implications for Venus geodynamics: Icarus, v. 123, p. 296–312.
———1998, Ribbon terrain formation, southwestern Fortuna Tessera, Venus: Implications for lithosphere evolution: Icarus, v. 132, p. 332–343.
Hansen, V.L., Willis, J.J., and Banerdt, W.B., 1997, Tectonic overview and synthesis, *in* Bougher, S.W., Hunten, D.M., and Phillips, R.J., Venus II: Geology, geophysics, atmosphere, and solar wind environment: Tucson, University of Arizona Press, p. 797–844.
Hauck, S.A., Phillips, R.J., and Price, M.H., 1998, Venus: Crater distribution and plains resurfacing models: Journal of Geophysical Research, v. 103, p. 13635–13642.
Head, J.W., and Basilevsky, A.T., 1998, Sequence of tectonic deformation in the history of Venus: Evidence from global stratigraphic relations: Geology, v. 26, p. 35–38.
Head, J.W., and Coffin, M.F., 1997, Large igneous provinces: A planetary perspective, *in* Mahoney, J.J., and Coffin, M.F., eds., Large igneous provinces: Continental, oceanic, and planetary volcanism: Geophysical Monograph Series: Washington, D.C., American Geophysical Union, p. 411–437.
Herrick, R.R., Sharpton, V.L., Malin, M.C., Lyons, S.N., and Feely K., 1997, Morphology and morphometry of impact craters, *in* Bougher, S.W., Hunten, D.M., and Phillips, R.J., Venus II: Geology, geophysics, atmosphere, and solar wind environment: Tucson, University of Arizona Press, p. 1015–1046.
Izenberg, N.R., Arvidson, R.E., and Phillips, R.J., 1994, Impact crater degradation on venusian plains: Geophysical Research Letters, v. 21, p. 289–292.
Kaula, W.M., 1990, Venus: A contrast in evolution to Earth: Science, v. 247, p. 1191–1196.
Keep, M., and Hansen, V.L., 1994, Structural evolution of Maxwell Montes, Venus: Implications for venusian mountain "belt" formation: Journal of Geophysical Research, v. 99, p. 26,015–26,028.
Kirk, R.L., Soderblom, L.A., and Lee, E.M., 1992, Enhanced visualization for interpretation of Magellan radar data—Supplement to the Magellan special issue: Journal of Geophysical Research, v. 97, no. E10, p. 16,371–16,380.
Kryuchkov, V.P., 1988, Ridge belts on the plains of Venus, in Abstracts submitted to the Nineteenth Lunar and Planetary Science Conference, March14–18, 1988: Houston, Lunar and Planetary Institute, p. 649–650.
McKenzie, D., Ford, P.G., Johnson, C., Parsons, B., Sandwell, D.T., Saunders, S., and Solomon, S.C., 1992, Features on Venus generated by plate boundary processes: Journal of Geophysical Research, v. 97, no. E8, p. 13,533–13,544.
Pavri, B., Head, J.W., Klose, K.B., and Wilson, L., 1992, Steep-sided domes on Venus: Characteristics, geologic setting, and eruption conditions from Magellan data: Journal of Geophysical Research, v. 97, no. E8, p. 13,445–13,478.
Phillips, R.J., and Hansen, V.L., 1998, Geological evolution of Venus: Rises, plains, plumes and plateaus: Science, v. 279, p. 1492–1497.
Plaut, J.J., 1993, Stereo imaging, *in* Ford, J.P., Plaut, J.J., Weitz, C.M., Farr, T.G., Senske, D.A., Michaels, G., Parker, T.J., Guide to Magellan image interpretation: Jet Propulsion Laboratory Publication 93–24, p. 33–41.
Sandwell, D.T., and Schubert, G., 1992a, Evidence for retrograde lithospheric subduction on Venus: Science, v. 257, p. 766–770.
———1992b, Flexural ridges, trenches, and outer rises around coronae on Venus: Journal of Geophysical Research, v. 97, no. E10, p. 16,069–16,084.
Schultz, P.H., 1992, Atmospheric effects on ejecta emplacement and crater formation on Venus from Magellan:Journal of Geophysical Research, v. 97, no. E10, p. 16,183–16,248.
Smrekar, S.E., and Stofan, E.R., 1997, Corona formation and heat loss on Venus by coupled upwelling and delamination: Science, v. 277, p. 1289–1294.
Squyres, S.W., Jankowski, D.G., Simons, M., Solomon, S.C., Hager, B.H., and McGill, G.E., 1992, Plains tectonism on Venus: The deformation belts of Lavinia Planitia: Journal of Geophysical Research, v. 97, no. E8, p. 13,579–13,599.
Stewart, E.M., and Head, J.W., 2000, Evidence for temporal continuity of deformation in the Baltis Vallis region of Venus from observations of canali topography, *in* Lunar and Planetary Science XXXI: Houston, Lunar and Planetary Institute, abstract #1692 [CD-ROM].
Stofan, E.R., Hamilton, V.E., Janes, D.M., and Smrekar, S.E., 1997, Coronae on Venus: Morphology and origin, *in* Bougher, S.W., Hunten, D.M. and Phillips, R.J., Venus II: Geology, geophysics, atmosphere, and solar wind environment: Tucson, University of Arizona Press, p. 901–930.
Stofan, E.R., Senske, D.A., and Michaels, G., 1993, Tectonic features in Magellan data, *in* Ford, J.P., Plaut, J.J., Weitz, C.M., Farr, T.G., Senske, D.A., Michaels, G., and Parker, T.J., Guide to Magellan image interpretation: Jet Propulsion Laboratory Publication 93–24, 93–108.
Stofan, E.R., Sharpton, V.L., Schubert, G., Baer, G., Bindschadler, D.L., Janes, D.M., and Squyres, S.W., 1992, Global distribution and characterisitics of coronae and related features on Venus: Implications for origin and relation to mantle processes: Journal of Geophysical Research, v. 97, p. 13347–13378.
Wilhelms, D.E., 1990, Geologic mapping, *in* Greeley, Ronald, and Batson, R.M., eds., Planetary mapping: New York, Cambridge University Press, p. 208–260.
Wood, J.A., 1997, Rock weathering on the surface of Venus, *in* Bougher, S.W., Hunten, D.M., and Phillips, R.J., Venus II: Geology, geophysics, atmosphere, and solar wind environment: Tucson, University of Arizona Press, p. 637–664.
Young, D.A., and Hansen, V.L., 2000, Initial mapping of the Rusalka Planitia quadrangle (V25), Venus, *in* Lunar and Planetary Science XXXI: Houston, Lunar and Planetary Institute, abstract #1622 [CD-ROM].

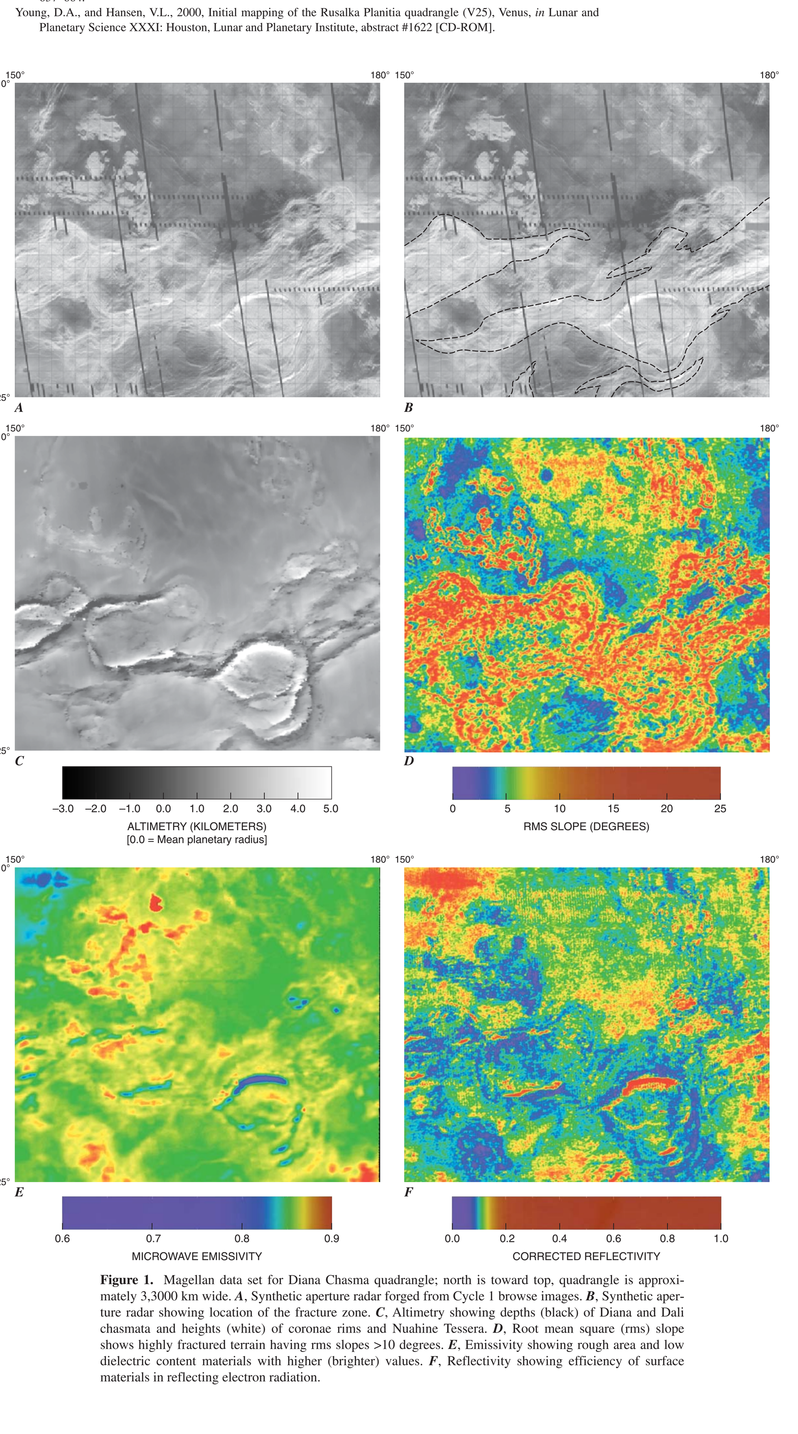

Figure 1. Magellan data set for Diana Chasma quadrangle; north is toward top, quadrangle is approximately 3,3000 km wide. ***A***, Synthetic aperture radar forged from Cycle 1 browse images. ***B***, Synthetic aperture radar showing location of the fracture zone. ***C***, Altimetry showing depths (black) of Diana and Dali chasmata and heights (white) of coronae rims and Nuahine Tessera. ***D***, Root mean square (rms) slope shows highly fractured terrain having rms slopes >10 degrees. ***E***, Emissivity showing rough area and low dielectric content materials with higher (brighter) values. ***F***, Reflectivity showing efficiency of surface materials in reflecting electron radiation.

Table 1. *Crater data for Diana Chasma quadrangle.*

Name	Latitude (° S.)	Longitude (° E.)	Diameter (km)	Unit location	Ejecta blanket	Impact halo	Central peak	Rim	Interior flooding	Deformation and notes
Alison	4.0	165.6	14.4	ba	Y	N	Y	Y	Y	None—partial interior flooding only; timing relations to wrinkle ridges unknown
Austen	25.0	168.4	45.1	cA	Y	N	Y	Y	N	Yes—ejecta covers Atahensik fractures but cut by fractures related to corona south of map area
Blanche	9.3	157.0	12.3	itb	Y	Y	N	Y	N	None—ejecta flows follow tessera structures and flow north, following current topography
Dheepa	21.6	176.3	4.7	fzcu	Y	Y	N	Y	N	None—ejecta flows follow preexisting fractures
Gulnara	23.7	174.0	5.0	cA	Y	N	N	N	N	Yes—highly degraded; post-dates fold formation
Langtry	17.0	155.0	50.3	cCBM	Y	N	N	Y2	Y	Yes—flooded interior heavily fractured; ejecta cut by fracture zone fractures
Leona	3.1	169.0	3.0	cES	Y	N	N	Y	N	None—ejecta deposited in broadly radial ray pattern; timing relations to wrinkle ridges unknown
Markham	4.1	155.6	71.8	cSe	Y	N	Y	Y	Y	None—extensive lava flows follow current topography, flow toward basin to the east; flows buttressed by wrinkle ridges and locally follow preexisting fractures
Martinez	11.7	174.7	23.5	cK	Y	N	Y	Y	Y	Yes—ejecta covers some fractures but not others; dark interior of crater cut by fractures; heavily deformed region makes delineation of discrete fracture set difficult
Patimat	1.3	156.5	5.1	cSe	Y	Y	Y	Y	N	None—diffuse wind-blown material thins to west; ejecta covers wrinkle ridges
Safarmo	10.8	161.4	7.4	cCBM	Y	N	Y	Y	N	Yes—ejecta locally cut by regionally late-forming NNE-trending fractures
Warren	11.7	176.5	50.9	cSi	Y	N	Y	Y	Y	Yes—heavily degraded and deformed ejecta blanket; interior flooding by two materials (radar bright and radar dark) exhibits small amounts of deformation
Zeinab	2.2	159.6	12.5	cES	Y	N	Y	Y	Y	None—flooded interior undeformed; timing relations to wrinkle ridges unknown
a	8.6	157.1	3.0	tN	P	N	N	P	--	Possible small crater
b	8.6	155.3	3.0	tN	P	N	N	P	--	Possible small crater
c	22.9	150.9	2.5	cCBM	Y	Y	N	Y	N	None—diffuse halo blankets surrounding structures
d	9.3	152.8	12.9	tN	N	N	N	P	Y	Possible small crater
	2.3	162.5	--	cES	N	N	N	N	N	Shock feature
	3.1	161.7	--	cES	N	N	N	N	N	Shock feature
	1.4	178.2	--	bb2	N	N	N	N	N	Shock feature
	24.9	153.0	--	cCBM	N	N	N	N	N	Shock feature

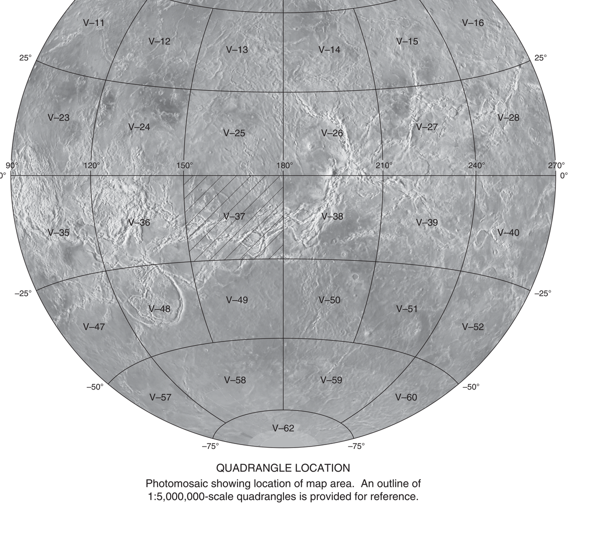

QUADRANGLE LOCATION
Photomosaic showing location of map area. An outline of 1:5,000,000-scale quadrangles is provided for reference.

GEOLOGIC MAP OF THE DIANA CHASMA QUADRANGLE (V–37), VENUS

By
Vicki L. Hansen and Heather R. DeShon
2002

Any use of trade, product, or firm names in this publication is for descriptive purposes only and does not imply endorsement by the U.S. Government

For sale by U.S. Geological Survey, Information Services, Box 25286, Federal Center, Denver, CO 80225, 1–888–ASK–USGS

ISBN 0-607-98067-2

Printed on recycled paper